Silica–Magnesia Support Composition Controls Metal Dispersion and Carbon Resistance in Ni-Catalyzed CO_2 Methanation

Authors

Min-Jae Kim[1*], Ji-Hoon Lee[2]

Affiliations

School of Chemical and Biological Engineering, Seoul National University, 1 Gwanak-ro, Gwanak-gu, Seoul 08826, Republic of Korea

***Corresponding author:** minjaekim@snu.ac.kr

Abstract

Ni-based catalysts are widely used for CO_2 methanation, but their activity and stability are strongly affected by metal dispersion and support basicity. In this study, mixed SiO_2–MgO supports with MgO contents from 10 to 70 wt% were prepared and loaded with 15 wt% Ni by impregnation. The catalysts were evaluated at 250–400 °C under H_2/CO_2 = 4. The Ni/SiO_4–MgO catalyst containing 40 wt% MgO achieved a CO_2 conversion of 78.5% and CH_4 selectivity of 98.1% at 350 °C, outperforming Ni/SiO_2 and Ni/MgO. CO_2-TPD showed that medium-strength basic sites increased from 94 to 276 μmol $gcat^{-1}$ after MgO incorporation, while TEM confirmed that the average Ni particle size decreased from 18.4 to 9.7 nm. A 100 h stability test showed only 4.6% activity loss, mainly due to improved carbon resistance on the mixed support.

Keywords: CO_2 methanation; Ni catalyst; SiO_2–MgO support; metal dispersion; support basicity; carbon resistance

1. Introduction

CO_2 methanation converts CO_2 and H_2 into CH_4 through the Sabatier reaction and provides a route for storing renewable energy in a form compatible with existing natural-gas infrastructure. The reaction is thermodynamically favored at relatively low temperature, whereas the kinetic activation of CO_2 remains difficult because of its high chemical stability. Increasing the reaction temperature accelerates CO_2 conversion but also promotes CO formation through the reverse water–gas shift reaction, thereby decreasing methane selectivity. Noble-metal catalysts such as Ru and Rh exhibit high activity at low temperature, but their cost and limited availability restrict large-scale application. Ni-based catalysts are therefore among the most widely investigated alternatives because Ni efficiently dissociates H_2, promotes hydrogenation of carbon-containing intermediates, and generally provides high CH_4 selectivity at substantially lower cost [1,2]. Nevertheless, conventional Ni catalysts frequently show insufficient activity in the moderate-temperature range and may gradually deactivate because of Ni particle growth, carbon

deposition, or unfavorable changes in the metal–support interface. Recent theoretical work on structurally diverse oxide–metal interfaces has further demonstrated that catalytic activity and deactivation behavior can vary markedly among different local interfacial configurations, indicating that the working catalyst is better described by an ensemble of accessible catalytic structures rather than by a single idealized active site [3]. This concept is particularly relevant to supported Ni catalysts, where the local coordination and chemical environment of Ni strongly depend on support composition, reduction state, and interfacial structure [4,5]. The support plays a central role in determining Ni dispersion, particle size, reducibility, CO_2 adsorption, and the stability of the metal phase under reaction conditions. SiO_2 is attractive because of its high surface area, thermal stability, and adjustable pore structure. These characteristics facilitate the preparation of highly dispersed Ni catalysts and provide relatively stable structural frameworks during methanation. However, the surface of SiO_2 contains only a limited number of basic sites, which restricts CO_2 adsorption and activation. Ni particles supported on silica may also migrate and grow during reduction or prolonged reaction, leading to a decrease in exposed metallic surface area. Smaller Ni particles generally provide a larger number of accessible metal sites and can substantially improve the methanation rate [6,7]. Various strategies have therefore been developed to stabilize highly dispersed Ni species on silica. Nickel silicate formation, confinement within mesoporous silica, and modification of the local Ni–SiO_2 interface can suppress metal agglomeration and improve dispersion [8,9]. Excessively strong Ni–SiO_2 interaction, however, may stabilize nickel silicate or strongly bound NiO species that are difficult to reduce, thereby decreasing the fraction of metallic Ni available for H_2 activation. The catalytic performance of silica-supported Ni consequently depends on a balance between structural stabilization and sufficient Ni reducibility. MgO offers a complementary set of properties because its surface contains basic oxygen sites that enhance CO_2 adsorption and can also restrict the migration of Ni species. Incorporation of MgO can therefore increase the local concentration of adsorbed CO_2-derived species while improving resistance to Ni sintering. However, NiO and MgO possess similar crystal structures and can form NiO–MgO solid solutions, particularly at high MgO content or after strong thermal treatment. Such interaction may stabilize Ni^{2+} species and make their reduction to catalytically active metallic Ni more difficult. The effect of MgO is therefore determined not only by the total number of basic sites but also by MgO loading, dispersion, interfacial contact with Ni, and the resulting Ni reducibility. Previous studies have shown that MgO addition can simultaneously modify Ni particle dispersion and the distribution of basic sites on silica-supported catalysts [10,11]. Increased CO_2 adsorption, however, does not necessarily produce higher methanation activity when the number of accessible metallic Ni sites becomes limited [12]. Ni–MgO boundary sites have also been associated with changes in reaction pathways and methane selectivity, showing that the catalytic function of MgO extends beyond simple enhancement of CO_2 adsorption [13]. Preparation-dependent differences in NiO–MgO interaction can further alter reduction behavior and low-temperature activity [14]. These observations indicate

that support basicity, Ni dispersion, reducibility, and interfacial structure are strongly coupled and must be considered together. Mixed SiO_2–MgO supports are attractive because they may combine the high surface area and structural stability of silica with the CO_2 adsorption capacity and basicity of MgO. In principle, silica can help maintain a porous structure and disperse Ni species, whereas MgO can provide additional basic sites and modify the electronic and structural environment near Ni particles. Similar concepts have been demonstrated for other mixed-oxide supports. SiO_2–ZrO_2 and Al_2O_3–ZrO_2 systems, for instance, can improve Ni dispersion, increase the density of CO_2 adsorption sites, and alter metal–support interaction relative to the corresponding single oxides [15,16]. The same principle may apply to SiO_2–MgO, but the catalytic response is unlikely to vary monotonically with MgO content. Weak basic sites may contribute little to CO_2 activation, whereas medium-strength sites can effectively adsorb and activate CO_2-derived species near hydrogenation centers. Excessively strong basic sites, in contrast, may stabilize carbonate species that react slowly and occupy surface sites for prolonged periods. Studies involving Mg–Al and related oxide supports likewise indicate that high methanation activity requires an appropriate balance between surface basicity and Ni reducibility rather than simply maximizing CO_2 uptake [17]. The spatial relationship between basic sites and metallic Ni is also important because CO_2 activation on the support must remain kinetically coupled to hydrogen activation and subsequent hydrogenation on nearby Ni sites. The composition of a mixed support can additionally influence catalyst deactivation. Ni sintering is promoted when metal particles are weakly anchored, whereas excessively strong Ni–support interactions can lower the amount of reducible Ni and suppress intrinsic activity. Carbon formation is similarly affected by particle size, local hydrogen availability, intermediate residence time, and surface basicity. Larger Ni particles may favor pathways leading to strongly adsorbed carbon species, while appropriate support basicity can facilitate adsorption and transformation of oxygen-containing intermediates. At the same time, very strong CO_2 adsorption may generate stable carbonate species and slow surface turnover. The long-term performance of Ni/SiO_2–MgO catalysts is therefore governed by several interdependent variables rather than by a single descriptor such as Ni particle size or total basicity. Previous stability studies have provided useful evidence for catalyst deactivation, but many tests have been limited to relatively short reaction times, and carbon resistance has often been inferred mainly from conversion loss rather than directly correlated with structural and surface properties [18]. Quantitative relationships among MgO content, Ni particle size, basic-site strength, carbon formation, and long-term methanation performance therefore remain insufficiently established.

A systematic study in which support composition is varied while Ni loading, preparation procedure, calcination conditions, and catalytic testing parameters are kept constant is required to isolate the role of the SiO_2/MgO ratio. The present work addresses this issue by preparing SiO_2–MgO supports containing 10–70 wt% MgO under identical synthesis conditions and loading each support with 15 wt% Ni. The resulting catalysts are designed to provide a controlled series in which changes in methanation behavior can be directly related to support composition rather than

to differences in Ni loading or preparation history. CO_2 temperature-programmed desorption is used to determine the distribution and strength of basic sites, while transmission electron microscopy is employed to quantify Ni particle size and dispersion. Catalytic performance is evaluated between 250 and 400°C to establish the relationship between support properties and low- to intermediate-temperature methanation activity, and a 100 h stability test is used to assess the resistance of the optimized catalyst to structural and carbon-related deactivation. By correlating MgO content with surface basicity, Ni accessibility, particle size, methane selectivity, and long-term stability, this study aims to identify the support composition that provides sufficient medium-strength basic sites for efficient CO_2 activation without sacrificing Ni reducibility or creating excessive NiO–MgO interaction. The broader significance of this work is to clarify how the chemical and structural functions of SiO_2 and MgO can be balanced within a mixed support, thereby establishing a composition–structure–activity relationship that can guide the rational design of stable and efficient Ni catalysts for low-temperature CO_2 methanation.

2. Materials and Methods

2.1 Catalyst Samples and Feed Gases

Nine Ni-based catalysts were prepared using SiO_2–MgO supports with different MgO contents. Seven mixed supports contained 10, 20, 30, 40, 50, 60, and 70 wt% MgO. Pure SiO_2 and MgO were used as reference supports. The mixed supports were prepared by co-precipitation from magnesium nitrate and sodium silicate solutions at 60 °C and pH 9.0. The precipitates were aged for 4 h, filtered, and washed with deionized water. They were then dried at 110 °C for 12 h and calcined at 600 °C for 5 h. Nickel was added by pore-volume impregnation using nickel nitrate hexahydrate. The nominal Ni loading was 15 wt% for all samples. The catalysts were dried at 110 °C and calcined at 500 °C for 4 h. Before testing, the samples were sieved to 250–425 μm. CO_2, H_2, N_2, He, and Ar with purities above 99.999% were used.

2.2 Reaction Design and Control Tests

CO_2 methanation was carried out in a stainless-steel fixed-bed reactor with an inner diameter of 8 mm. Each test used 0.30 g of catalyst mixed with 0.60 g of quartz particles. Before reaction, the catalyst was reduced in 20 vol% H_2/N_2 at 500 °C for 3 h. The reactor was then cooled to the selected reaction temperature. Tests were conducted between 250 and 400 °C at 1.0 MPa. The H_2/CO_2 molar ratio was fixed at 4, and the gas hourly space velocity was 12,000 mL g_cat^{-1} h^{-1}. Ni/SiO_2 and Ni/MgO were used as control catalysts. These samples were used to separate the effects of SiO_2 and MgO. All mixed-support catalysts were tested at the same Ni loading and under the same reaction conditions. Blank tests with quartz and unloaded supports produced no measurable CH_4. The catalyst containing 40 wt% MgO was tested for 100 h at 350 °C to assess stability.

2.3 Measurement Methods and Quality Control

Crystal phases were identified by X-ray diffraction with Cu Kα radiation. Surface area and pore volume were measured by N_2 adsorption at −196 °C. The actual Ni and Mg contents were measured by inductively coupled plasma optical emission spectroscopy. Ni particle sizes were determined by transmission electron microscopy. At least 150 particles from different sample areas were measured for each catalyst. CO_2 temperature-programmed desorption was carried out after CO_2 adsorption at 50 °C. The sample was then heated to 700 °C in He. H_2 temperature-programmed reduction was measured from 50 to 800 °C in 10 vol% H_2/Ar. Carbon on the spent catalysts was measured by thermogravimetric analysis in air. Reaction products were analyzed by online gas chromatography with thermal-conductivity and flame-ionization detectors. Gas flow meters were calibrated before each test series. Carbon balances were kept between 96% and 104%. Each catalytic test was repeated three times. Tests with a relative error above 5% were repeated.

2.4 Data Processing and Model Equations

CO_2 conversion was calculated from the inlet and outlet molar flow rates:

$$X_{CO_2}=\frac{F_{CO_2,in}-F_{CO_2,out}}{F_{CO_2,in}}\times 100\%$$

where $F_{CO_2,in}$ and $F_{CO_2,out}$ are the inlet and outlet CO_2 molar flow rates, respectively. CH_4 selectivity was calculated on a carbon basis:

$$S_{CH_4}=\frac{F_{CH_4}}{F_{CH_4}+F_{CO}}\times 100\%$$

where F_{CH_4} and F_{CO} are the outlet molar flow rates of CH_4 and CO, respectively. CO_2-TPD peaks were divided into weak, medium, and strong basic-site regions according to desorption temperature. Mean Ni particle size was calculated from the number-based particle-size distribution. Multiple linear regression was used to examine the relation between the CH_4 formation rate and catalyst properties. The input variables were Ni particle size, medium-strength basic-site density, surface area, and H_2 uptake.

2.5 Kinetic, Stability, and Statistical Analysis

Kinetic measurements were started after the product composition remained stable for at least 2 h. Apparent activation energies were calculated from reaction rates measured between 250 and 310 °C. CO_2 conversion was kept below 15% to reduce heat- and mass-transfer effects. External mass transfer was checked by changing the total gas flow from 60 to 140 mL min^{-1}. Internal diffusion was tested with catalyst particle sizes of 150–250, 250–425, and 425–600 μm. No clear rate difference was found between the two smaller particle ranges. Catalyst deactivation during the 100 h test was calculated from the decrease in CO_2 conversion. Pearson correlation analysis was used to compare activity with Ni particle size, basic-site density, H_2 uptake, and carbon amount.

Differences among catalyst samples were tested by one-way analysis of variance followed by Tukey's test. Differences were considered significant at $p<0.05$. Results are reported as the mean ± standard deviation of three independent tests.

3. Results and Discussion

3.1 Effect of Support Composition on CO_2 Methanation

The MgO content strongly affected CO_2 conversion and CH_4 selectivity. Ni/SiO_2 gave a CO_2 conversion of 51.3% and a CH_4 selectivity of 91.6% at 350 °C. Adding 10–40 wt% MgO increased both values. The catalyst with 40 wt% MgO gave the best performance, with a CO_2 conversion of 78.5% and a CH_4 selectivity of 98.1%. Further MgO addition reduced the conversion. The catalyst with 70 wt% MgO reached 66.4%, while Ni/MgO reached 60.8%. The activity therefore showed a volcano-shaped trend with MgO content. Low MgO contents did not provide enough basic sites for CO_2 adsorption. High MgO contents formed more Ni species that were difficult to reduce. The reaction results and 100 h stability test are shown in Fig. 1. Nyambura et al. (2026) also found that mixed SiO_2–MgO supports improved CH_4 selectivity. However, their best support ratio differed from that in the present study. This difference may result from changes in Ni loading, pore structure, support preparation, and reduction conditions [19,20].

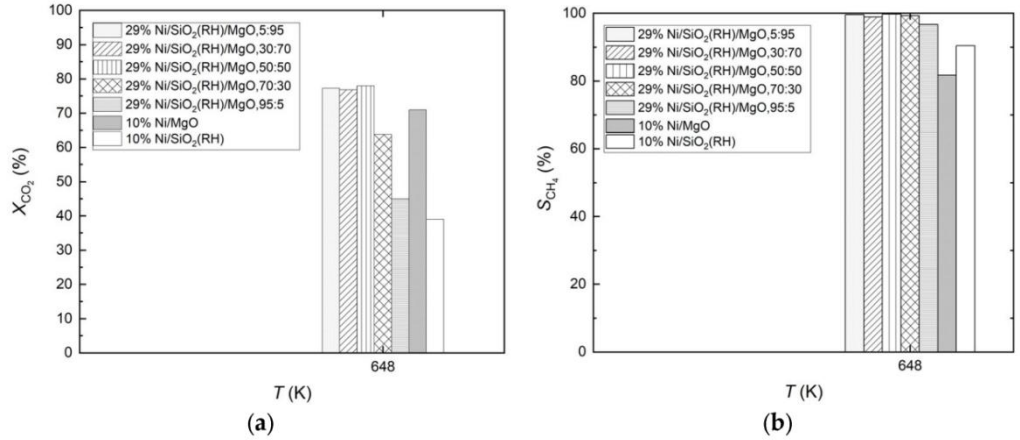

Fig. 1. CO_2 conversion, CH_4 selectivity, and stability of Ni/SiO_2–MgO catalysts with different MgO contents.

3.2 Basic Sites and Ni Reduction

CO_2-TPD showed that MgO changed the number and strength of the basic sites. Ni/SiO_2 contained 94 μmol g_cat^{-1} of medium-strength sites. This value increased to 276 μmol g_cat^{-1} for Ni/40MgO–SiO_2. These sites adsorbed CO_2 at the reaction temperature and supplied carbonate or formate species for CH_4 formation. Catalysts with 50–70 wt% MgO contained more strong basic sites. However, these sites did not further improve the reaction rate. CO_2 may have formed stable carbonate species that reacted slowly. H_2-TPR showed that high MgO contents shifted the main

NiO reduction peak to higher temperatures. This shift indicates stronger NiO–MgO contact and a lower amount of metallic Ni after reduction. Abir et al. (2026) reported a similar trend. MgO improved Ni dispersion but also formed strongly bound Ni species. The present results show that medium-strength basic sites were more closely related to CO_2 conversion than total basicity [21,22].

3.3 Ni Dispersion and Carbon Formation

TEM showed that the mean Ni particle size decreased as the MgO content increased to 40 wt%. Ni/SiO_2 had an average Ni particle size of 18.4 nm, while Ni/40MgO–SiO_2 had a value of 9.7 nm. The mixed support limited Ni movement during calcination and reduction. It also produced a narrower particle-size range. Above 40 wt% MgO, the Ni particle size changed only slightly, but the amount of easily reduced Ni decreased. Thus, small Ni particles alone did not explain the activity trend. Poosri et al. (2026) also found that smaller Ni particles increased the number of active sites on Ni/SiO_2. In the present study, Ni dispersion worked together with basicity and reducibility. TGA showed 2.8 wt% carbon on spent Ni/SiO_2 and only 0.7 wt% on Ni/40MgO–SiO_2. The mixed support improved CO_2 adsorption near the Ni particles and reduced the build-up of stable carbon deposits [23,24]. The CO_2-TPD profiles, Ni particle-size distributions, and carbon contents are shown in Fig.2.

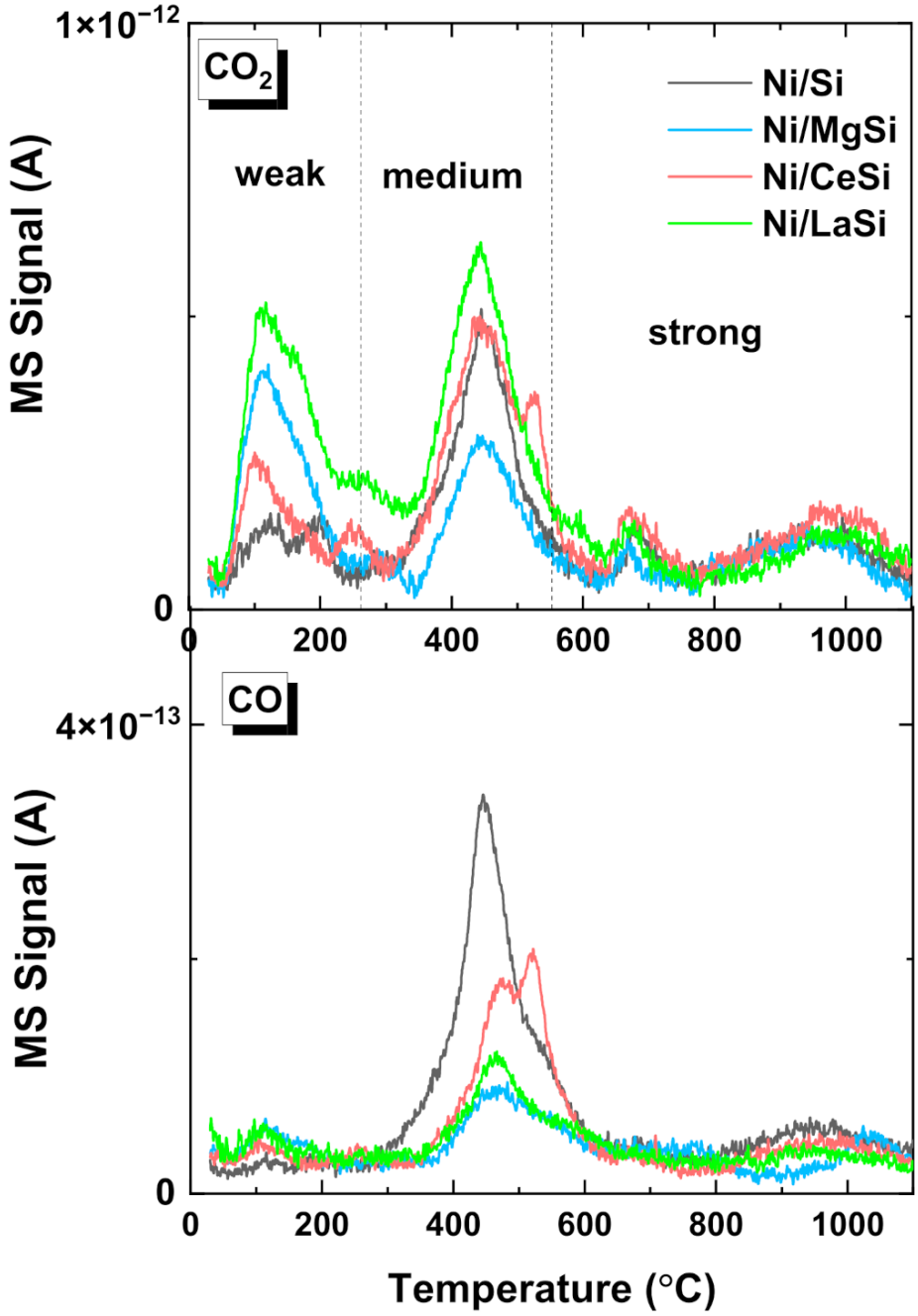

Fig. 2. Basic sites, Ni particle size, and carbon deposits on fresh and spent Ni/SiO_2–MgO catalysts.

3.4 Stability and Relation between Structure and Activity

Ni/40MgO–SiO_2 lost only 4.6% of its initial activity during the 100 h test at 350 °C. CH_4 selectivity remained above 97.5%. By comparison, Ni/SiO_2 lost 15.2% of its activity after 60 h. The mean Ni particle size on the optimized catalyst increased from 9.7 to 11.2 nm after reaction. The value for Ni/SiO_2 increased from 18.4 to 25.6 nm. These results show that the mixed support reduced Ni particle growth. The CH_4 formation rate was positively related to the amount of medium-strength basic sites, with R^2=0.88. Negative relations were found with Ni particle size

(R^2=0.81) and carbon content (R^2=0.86). Surface area showed only a weak relation with activity. Aouadi et al. (2026) also reported that surface area alone could not explain CO_2 methanation activity. Ni dispersion, basicity, reducibility, and metal–support contact were more important. The 40 wt% MgO support gave the best balance among these properties. Higher MgO contents increased basicity but reduced the amount of active metallic Ni.

4. Conclusion

The SiO_2–MgO ratio strongly affected Ni particle size, CO_2 adsorption, carbon formation, and methanation performance. The catalyst with 40 wt% MgO showed the highest activity. It reached 78.5% CO_2 conversion and 98.1% CH_4 selectivity at 350 °C. MgO addition increased the number of medium-strength basic sites from 94 to 276 μmol g_cat^{-1}. It also reduced the mean Ni particle size from 18.4 to 9.7 nm. These changes improved CO_2 adsorption and increased the number of exposed Ni sites. During the 100 h test, the optimized catalyst showed only a 4.6% loss in activity and formed less carbon than Ni/SiO_2. However, excess MgO produced more strongly bound Ni species and lowered the amount of metallic Ni available for H_2 activation. The results show that high methanation activity depends on a suitable balance among basicity, Ni dispersion, and Ni reduction. This finding may support the design of stable Ni catalysts for renewable methane production. The study was limited to laboratory tests and one Ni loading. Future work should examine larger catalyst batches, longer test periods, different Ni contents, and feeds containing water or common gas impurities.

References

1. Chen, F., Liang, H., Li, S., Yue, L., & Xu, P. (2025). Design of Domestic Chip Scheduling Architecture for Smart Grid Based on Edge Collaboration.

2. Nyambura, S. M., Yong, Y. C., Li, H., Li, C., Tang, W., Liu, M., ... & Fui Chin, B. L. (2026). Nickel-based catalysts for plastic pyrolysis: advances in product selectivity, yield optimization, and emerging pathways for thermochemical recycling. Journal of Materials Chemistry A, 14(11), 6145-6174.

3. Yang, Z., Alexandrova, A. N., & Sautet, P. (2026). Modeling CO2 Hydrogenation to Methanol on an Ensemble of Inverse ZrO2 on Cu Catalytic Sites: Mechanism, Reactivity, and Deactivation. Angewandte Chemie, e5448247.

4. Park, H. R., Kim, B. J., Ryu, S. J., Jeon, B. H., & Roh, H. S. (2026). Selective phase exposure induces Ni–Ce interfacial redox reconstruction for CO2 activation. Journal of Materials Chemistry A.

5. Liang, R., Feifan, F. N. U., Liang, Y., & Ye, Z. (2025). Emotion-Aware Interface Adaptation in Mobile Applications Based on Color Psychology and Multimodal User State Recognition. Frontiers in Artificial Intelligence Research, 2(1), 51-57.

6. Bao, Y., Qiu, Y., & Wang, H. (2026, May). Unified Identity Layer for Hyperscale Ecosystems: A Framework for Cross-Platform User Attribution and Experimentation. In 2026 6th International Conference on Machine Learning and Intelligent Systems Engineering (MLISE) (pp. 540-543). IEEE.

7. Abir, M. A., Kulkarni, M., Phillips, R. E., Harrah, J. Z., & Ball, M. R. (2026). Spectroscopic investigation of the influence of Ni particle size in CO2 methanation. Nanoscale, 18(5), 2766-2779.

8. Du, Y. (2025). Research on Digital Quality Traceability System for Temperature-Controlled Supply Chain of Foreign Trade Wine Driven by Blockchain and IoT. Business and Social Sciences Proceedings, 4, 57-65.

9. Abdulai, Y. (2025). Synthesis of Hierarchical Zsm-5 Zeolites with Unique Morphologies and Tunable Sio2/al2o3 Ratios for Dry Reforming of Methane (Doctoral dissertation, King Fahd University of Petroleum and Minerals).

10. Jiao, Y., Zhao, B., Wang, A., & Shi, T. (2026). Construction and Empirical Study of a Modularized Teaching System for Art Courses Based on a Unified Training Pathway.

11. Poosri, P., Phichairatanaphong, O., Witoon, T., Chareonpanich, M., & Donphai, W. (2026). Silica-anchored cerium-magnesium supported nickel toward improved CO2 reforming of CH4. Molecular Catalysis, 592, 115722.

12. Yang, J. (2026). Stage-Coupled Computational Framework for Stratified Accessibility and Equity Analysis in Community-Based Elderly Care Services.

13. Aouadi, A., Nesrat, H. S., Aouadi, S., Bouafia, A., Saoud, D. H., Laouini, S. E., ... & Zelca, Z. (2026). Defect-engineered MgO nanoparticles with high surface area for integrated solar-driven CO2 reduction and hydrogen generation. Ionics, 32(3), 3103-3121.

14. Wu, J., Wu, D., Zhang, J., & Peng, Y. (2026). Generative AI Feedback in Junior High School Artistic Creation Evaluation. Available at SSRN 7244838.

15. Najari, S., Saeidi, S., Sápi, A., Kónya, Z., & Somorjai, G. A. (2025). Unveiling the power of proximity of prevalent Fe-based tandem catalysts in CO2 hydrogenation via modified Fischer–Tropsch: crucial relations toward industrialization. Chemical Reviews, 125(21), 10179.

16. Gu, X. (2026). Identifying Causal Effects and Analyzing Heterogeneity of User Growth Interventions on Digital Platforms: Evidence from Large-Scale Behavioral Data. Available at SSRN 6809181.

17. Bravo, L. M. (2025). Exploring Support Effects, Promoter Integration, and Adsorption and Reaction Kinetics in Multi-Metal Catalysts and Dual Function Materials for the Advancement of CO2 Capture and Hydrogenation Technologies. McGill University (Canada).

18. You, S. (2026). Verifiable Audit Mechanisms in AI Compliance Automation: Scalability. Available at SSRN 6547458.

19. Sedtabute, S., Vitidsant, T., & Ngamcharussrivichai, C. (2025). Production of jet fuel-range bio-hydrocarbons over nickel-based catalysts through hydrothermolysis without external H2: Effect of nanoporous supports. Energy Conversion and Management, 331, 119679.
20. Kosari, M., O'Brien, C., Yang, K., Mei, Y., Hondos, E., Xi, S., ... & Li, F. (2025). Bimodal hierarchically porous SiO2 sphere-supported catalysts for dry reforming of methane. ACS Catalysis, 15(16), 14317-14330.
21. Jiao, Y., Shi, T., Zhao, B., & Wang, A. (2026). The Impact of VR Sketching Simulations on the Assessment of Scale and Site Suitability in Public Art Spaces.
22. Liang, S., Zhang, X., Du, Y., & Chen, W. (2026). Supply Network Restructuring and Capacity Ramp-Up Limits in the Localized Expansion of High-Performance Computing Equipment Production. Available at SSRN 7339738.
23. Alshammari, D. A., Aladeemy, S. A., Ali, R. M., Marouani, M. E., El-Naggar, N. A., Alharbi, F. S., ... & Al-Fatesh, A. S. (2026). A comparative study of SiO2, Al2O3, and mixed SiO2-Al2O3-supported nickel catalysts for dry reforming of methane: effects of calcination temperature on catalytic performance. Journal of Materials Science, 61(2), 834-853.
24. Bao, Y., & Wang, H. (2026). Edge-to-Cloud Infrastructure Continuum: A Unified Framework for Optimizing Industrial IoT Systems. Available at SSRN 7185578.